Fabró Ferran (Orcid ID: 0000-0002-5448-3357)

Montanya Joan (Orcid ID: 0000-0003-2488-697X)

van der Velde Oscar A. (Orcid ID: 0000-0002-1638-6628)

Pineda Nicolau (Orcid ID: 0000-0002-2507-8424)

Williams Earle R. (Orcid ID: 0000-0003-1488-3361)

On the TGF/lightning ratio asymmetry

Ferran Fabró[1], Joan Montanyà[1], Oscar A. van der Velde[1], Nicolau Pineda[2], Earle R. Williams[3]

[1]Polytechnic University of Catalonia, Terrassa, Spain

[2]Meteorological Service of Catalonia, Barcelona, Spain

[3]Massachusetts Institute of Technology, Boston, Massachusetts, USA

Corresponding author: Ferran Fabró (ferran.fabro@upc.edu)

Key Points:

- Drier surface and high CAPE in Africa allows for stronger updrafts, and large concentrations of aerosols enhance electrification processes
- Thunderstorms in Africa may have intense electrification but charge regions are elevated in the atmosphere and closer to each other
- Thunderstorms in Africa, do not accomplish the favorable conditions for TGF production

This article has been accepted for publication and undergone full peer review but has not been through the copyediting, typesetting, pagination and proofreading process which may lead to differences between this version and the Version of Record. Please cite this article as doi: 10.1029/2018JD030075

Abstract

Africa is one of the most productive lightning regions on Earth, yet it has a lower TGF-to-lightning ratio especially compared with Central America. In this paper we have analyzed the global distribution of different meteorological parameters in order to explain the TGF/lightning ratio asymmetry. We show here that a drier surface and larger CAPE in Africa may produce thunderstorms with intense electric charge regions but elevated in the atmosphere and closer to each other, which allows for higher flash rates and less energetic, shorter and smaller flashes. The results we present here suggest that continental thunderstorms in Africa more rarely fulfill the lightning and thundercloud requirements for TGF production inferred from observations and models.

1 Introduction

Terrestrial Gamma ray Flashes (TGFs) are very brief and very intense bursts of gamma rays produced in the atmosphere (Fishman et al. 1994). TGFs are the most energetic natural radiation produced on Earth, with durations below 1 ms and energies up to 100 MeV (Tavani et al. 2011). Further satellite missions, although they have not been designed specifically for the study of TGFs, have been used for that purpose: the Reuven Ramaty High-Energy Spectroscopic Imager (RHESSI) (Smith et al. 2005), the Astrorrivelatore Gamma ad Immagine Leggero (AGILE) (Marisaldi et al. 2010) and the Fermi Space Telescope (Briggs et al. 2010). Simulations of gamma rays propagating through the atmosphere have established the source below 21 km of altitude (Dwyer and Smith, 2005, Ostgaard et al. 2008) and the analysis of the data detected by these instruments revealed that TGFs are produced within thunderstorms at mid-tropospheric altitudes (Cummer et al., 2014). Williams (2006) proposed that TGF may be produced by intra-cloud (IC) upward negative leaders, which is supported by the observations of TGFs correlated with individual lightning (Cummer et al. 2005, Stanley et al. 2006, Connaughton et al. 2010) and more specifically with negative upward leaders (Lu et al, 2010, Shao et al. 2010, Ostgaard et al. 2013, Cummer et al. 2014, 2015).

The origin of the gamma rays in the TGFs is due to bremsstrahlung radiation that results from the interaction of runaway electrons with air molecules. Runaway electrons are produced when energy gain due to the acceleration in the strong electric fields of thunderstorms exceeds energy losses (Wilson, 1925). If electrons collide with air molecules creating secondary electrons which can also runaway, an avalanche of high energy electrons is created. This process is known as Relativistic Runaway Electron Avalanche (RREA) (Gurevich 1992). Two theories are nowadays widely accepted to explain the production mechanism of TGFs. The first theory proposes that free electrons can run away in the very strong electric fields created in the tip of lightning leaders (Moss et al. 2006, Dwyer 2008, Carlson et al. 2010, Dwyer et al. 2010, Celestin 2012). This mechanism is based on the thermal runaway proposed by Gurevich (1961). The second theory is the relativistic feedback model (Dwyer 2012, Liu and Dwyer 2013). It proposes that RREA is augmented by the positive feedback mechanism in order to create the fluxes of electrons that produce the gamma-rays observed in the instruments on-board satellites. The electrons are accelerated in the large-scale electric field between the main positive and negative charge centers of thunderclouds or in the electric field created by lightning or most likely a combination of the two.

Since TGFs are produced within thunderstorms and correlated with lightning, some studies have tried to find out if there are prevalent meteorological conditions conducive to

TGF production. There is a very good agreement between seasonal, diurnal and geographical TGF and lightning occurrence, clearly dominated by the three lightning chimneys: Africa, South America and Southeast Asia (Splitt et al. 2010). Tropical Africa is also the region in Earth with the greatest occurrence of Mesoscale Convective Systems (MCS) with very strong convection and lightning flash rate (Toracinta and Zipser, 2001). Africa, and more specifically the Congo basin, is the lightning hotspot of the planet (Christian et al., 2003). That seems to indicate that Africa should be the region with the higher TGF production. Contrary to what one may expect, as shown in different publications (Smith et al. 2010, Fuschino et al. 2011, Briggs et al. 2013), the TGF/lightning ratio in Africa is lower in comparison with South America and Southeast Asia. For AGILE, the TGF/lightning ratio (normalized to the value in central America) are 1 for central America, 0.4 for Africa and 0.5 for Southeast Asia (Fuschino et al., 2011) while for Fermi, the TGF/lightning ratio (normalized to the value in Americas) are 1 for Americas, 0.47 for Africa and 0.55 for Asia (Briggs et al., 2013). Therefore, there is an asymmetry in the TGF/lightning ratio. Smith et al. (2010) suggested that there may be meteorological differences between coastal and inland regions that could explain the TGF/lightning ratio asymmetry. Other publications show that TGFs are associated with tall tropical thunderstorm systems (Splitt et al., 2010) and with high values of CAPE and liquid water content (Fabró et al. 2015). Barnes et al. (2015) found that thunderstorms associated with TGFs have larger concentrations of cloud water, cloud ice, precipitation water and precipitation ice. However, Chronis et al. (2016) analyzed 24 TGF-producing storms for CAPE and different NexRAD products used to measure convection, and did not find any specific characteristic preferred for TGF production.

RHESSI, AGILE and Fermi have very different orbital inclinations, but all three show very clearly that the lowest and highest TGF/lightning ratio in the tropics are achieved in Africa and America respectively. The objective of this investigation is to identify meteorological factors that make a difference in the lightning production that may have direct implications in TGF production, focusing the analysis in African and Central American lightning chimneys. On this basis, we propose a hypothesis consistent with the TGF production mechanisms that may explain why the TGF/lightning ratio in Africa is the least among three chimneys.

2 Data and methodology

This study relies mainly on the African and Central American TGF production regions. These regions identified by Smith et al. (2010) with deficits and excess with respect to the TGF/lightning ratio are highlighted in the Figure 1. Continental Africa, was identified by Smith et al. (2010) as the lighting chimney with a deficit in the TGF/lightning ratio, is highlighted in red, while the regions in Central America with a higher TGF/lightning ratio are highlighted in black. We will refer to these two regions as Af and CA respectively.

2.1 Meteorological reanalysis

In order to compare characteristic meteorological parameters related with thunderstorms in the three regions, we have analyzed meteorological data from the ERA-Interim reanalysis (Dee et al., 2011) for the period 2010-2013. The parameters analyzed are: Total column Liquid Water content (TCLW), Total column Water Vapor content (TCWV), Total column

Ice Water content (TCIW), 2-meter temperature and Convective Available Potential Energy (CAPE). ERA-Interim data is given in 6h-periods (4 per day at the beginning of each period, that is at 00, 06, 12 and 18 UTC) with 1º × 1º resolution. That means that for each parameter, the data for the whole period of 4 years (1461 days) is given in matrix of 181x360x5844 elements (lat x lon x time). Then, for each of the 1º × 1º elements of every parameter we have computed the median and the 90th percentile, but only for 6h-period time elements considered under thunderstorm conditions. In order to find these conditions, we have used lightning data of the Very Low Frequency (VLF) lightning detection network called World Wide Lightning Location Network (WWLLN) (Rodger et al. 2006). It has been considered that the 6h-periods time elements under thunderstorms conditions must satisfy a number of WWLLN stroke detections > 1. The result are two matrixes of 181 × 360 corresponding to every 1º×1º region with the median (50th percentile) (P50) and 90th percentile (P90) respectively of each parameter that has been represented in the maps plotted in the figures 2-6. These maps are useful to identify mean values (P50 maps) and extreme values (P90 maps) of the parameters analyzed. As pointed out previously, for each 6h-period the data is given at the beginning of the period what means that results presented here are representative of the pre-convective environment.

On the other hand, we have also computed boxplots, P50 and P90 for the three regions highlighted in the Figure 1 for the whole period analyzed (see Supporting Information document). We have also computed seasonal maps, boxplots and P50 and P90 corresponding to northern hemisphere meteorological seasons winter (December – January - February, DJA), spring (March – April – May, MAM), summer (June – July – August, JJA) and autumn (September – October – November, SON) in order to take into account the effect of intertropical convergence zone (ITCZ) seasonal migration (Asnani, 1993). Here we present P50 and P90 values for the four seasons (maps and boxplots can also be found in the Supporting Information document).

2.2 NASA Earth Observations

Aerosol concentration is known to be a key factor in the electrification of thunderstorms (Mansell and Ziegler 2013, Zhao et al. 2015). We have reviewed monthly global maps from NASA Earth Observations[1] (NEO) of atmospheric optical thickness (AOT) which gives an idea of the concentration of aerosols like dust, smoke from fires, volcanic ash, sea salts and pollution from factories. In this case, we have computed maps of AOT for the same four seasons DJF, MAM, JJA and MAM seasons for the period 2010 – 2013. We have also plotted in this maps all the TGFs detected by Fermi in the period 2008 – 2016[2] and the regions with LIS-OTD flash density > 40 flashes/ km^2·year (Figures 7, 8, 9 and 10).

3 Results

The analysis of the results is focused on Africa as the region of interest because it is the one with the highest lightning activity (Christian et al 2003, Cecile et al. 2014, Beirle et al. 2014) and the one with the lowest TGF/lightning ratio, in comparison with CA because it is the one with the highest TGF/lightning ratio (Smith et al. 2010, Fuschino et al. 2011, Briggs et al. 2013). These regions are also identified in the Figures 2-6 as in the Figure 1. The values

[1] https://neo.sci.gsfc.nasa.gov
[2] https://fermi.gsfc.nasa.gov/ssc/data/access/gbm/tgf/
[3] https://ghrc.nsstc.nasa.gov/lightning/data/data_lis_vhr-climatology.html

of the median and 90th percentile are summarized in Table 1. The values of the median and 90th percentile for the DJF - MAM and JJA – SON are summarized in Table 2 and Table 3 respectively.

3.1 Temperature

There is no significant difference in the surface 2-meter temperature among the two TGF production regions analyzed here, Africa and Central America, as can be observed in table 1, 2 and 3, except the P90 that is clearly high in Africa in the season DJF and MAM (table 2). On the other hand, in figure 2.a it can be observed that the SA regions are surrounded by ocean with higher 2-meter temperature while the region in Africa with high TGF production is far from the ocean. Moreover, in both Figures 2.a and 2.b we can see that the region of interest in Africa is also the one with the highest 2-meter temperature extreme values.

3.2 CAPE

Figures 3.a and 3.b present the maps corresponding to CAPE, and it can be observed that is higher in Africa (Table 1). In the DJF and MAM seasons, CAPE is also higher in Africa (Table 2), however in the JJA season is higher in Central America while in SON seasons is comparable in both regions, Africa and Central America (Table 3). Moreover, the region in Africa with CAPE above 1500 J/kg (Figure 3.b) is clearly larger in comparison with SA.

3.3 Water content

Here we present together the results for the Total Column Liquid Water content (Figure 4.a-b), the Total Column of Ice Water content (Figure 5.a-b) and the Total Colum Water Vapor content (Figure 6.a - b). These maps indicate the available water content in every region. Figures 4.a and 4.b show that the inland region of interest in Africa has low values of liquid water content while the higher values are achieved in the southern coast of Costa Rica and Panama and the western coast of Colombia. The amount of ice water content represented in Figures 5.a and 5.b presents a similar geographical distribution to the previous one (Figure 4.a-b), being the lowest concentration in the region of interest in Africa. In Figure 6 it can be seen very clearly that the amount of water vapor is very high and quite constant along the tropics except for the inland region of interest in Africa. Finally, from the observation of the 6 maps (Figures 4.a to 6.b) and the values of P50 and P90 summarized in Tables 1, 2 and 3 we can establish that inland regions are drier than coastal regions and that the region of interest in Africa is the driest of the two TGF production regions for the four seasons analyzed.

3.4 Atmospheric optical thickness and carbon monoxide concentration

The atmospheric optical thickness graphics in Figures 7 and 8 is very useful because it gives an idea of aerosol concentration in the atmosphere such as dust, smoke from fires, volcanic ash, sea salt and pollution from factories. We have plotted this parameter because, as pointed out by Williams (2005a), a more polluted boundary layer can enhance ice-based electrification processes. As previously stated, we present atmospheric optical thickness for the DJF, MAM, JJA and SON seasons (Figures 7-10) for the period 2010 – 2013. In the same

graphics we have also plotted TGFs detected by Fermi from 2008 to 2016 and regions with TRMM LIS flash density > 40 flashes/km^2·year in the period from 1998 to 2013, also for the respective seasons. Here we only present this plots for Africa because atmospheric optical thickness is clearly high in Africa compared to Central America (see Supporting Information document). In the Figures 7 and 8 corresponding to DJF and MAM it can be observed that the region in central Africa with high flash density it has also high values of AOT, however the concentration of TGFs detected by Fermi is comparable to the southern region with low flash density and low AOT. In both cases, the concentration of TGFs to the West of the high flash density region in Central Africa, where the AOT is very high, is very low. The flash density in this region is always > 10 flashes/km^2·year (Albrecht et al., 2016), and in the case of MAM season, it is even above 40 flashes/km^2·year

In the Figure 9, the JJA season, it can be observed that almost all the TGFs occur within the region with high flash density, however the TGF concentration is high in the region with low AOT. Finally, for the SON season it can be observed in the figure 10 that the TGF occurrence is high in the region with the high flash density, indistinctly of the AOT. The concentration of TGFs to the South and West of central Africa where AOT is very low and flash density flash density > 10 flashes/km^2·year is also considerable.

4 Discussion

It was revealed that the region of interest in Africa has lower concentrations of liquid water, ice water and water vapour. This indicates that this region is drier than CA, consistent with previous work (Meyer et al. 2007, Karlson et al. 2013). According to Williams (2005a), a drier surface allows for a deeper reservoir of unstable air. That agrees with the higher values of CAPE observed in the region of interest Africa reported in the previous section. The only season with values CAPE clearly lower in Africa than in CA is JJA. Therefore, the right conditions for the existence of strong updrafts are more common in Africa. Different publications have already shown that Africa is the region with the stronger deep convection (Matsui et al. 2016) and the tallest hot towers (Liu and Zipser, 2005, Liu et al. 2008), which are direct consequences of strong updrafts. Marshall et al. (1995) measured vertical electric field by the use of balloon soundings, and the results support the hypothesis presented by MacGorman (1989) that strong updrafts elevate charge regions. This hypothesis is confirmed by Stolzenburg et al. (1998), who notice that the main negative charge is elevated when updraft speed increases, and later by Guo et al. (2016), who reported that the height of charge regions is correlated with the strength of the updraft.

In order to understand the implications of an elevated negative charge region we have computed a simple model of the thundercloud electric field (Riousset et al. 2007, Krehbiel 2008). We have assumed a thundercloud electric charge structure based on Riousset et al. (2007), with four charge regions that are considered to be uniformly charged disks, but taking altitudes of the charge regions from Lightning Mapping Array measurements in Colombia from López et al. (2018). The dimensions and charge of the disks are specified in the Table 4 and is represented in the Figure 12.a. For each charge region, the altitude corresponds to the centre of the disk and depth corresponds to the vertical extent.

We have computed 19 different cases in which the altitudes of the main negative and the lower positive charge regions was increased in 100 m steps successively, while the altitudes of the main positive and upper negative charge regions remain constant. That is, for the main negative charge region from 6.5 km to 8.4 km altitude and for the lower positive charge region from 4.25 km to 6.15 km of altitude. Then, for the 19 different cases we have calculated the minimum charge density in the regions in order to achieve the lightning initiation field (E_{init}=2.16·10^5 V/m · *n*, being *n* the density of air with respect to that at sea level, Riousset et al. 2007) between the main negative and main positive charge regions. This initiation field can be considered the same than the threshold field (E_{th}) for both negative and positive to propagate in intracloud discharges (Riousset et al. 2007). The results are presented in Figure 11. Vertical charge structure, electric field and potential corresponding to cases with charge separation of 1900 m and 400 m are respectively plotted in Figures 10 and Figure 11.

These results shows that when the negative charge region is elevated, less charge is needed for lightning initiation and positive and negative leaders propagation. That means, that under the same conditions, in terms of charging rate, thunderstorms with an elevated main negative charge region will be more often discharged and the IC activity will be greater. This is consistent with Guo et al. (2016), who reported that strong updrafts favour IC activity, and publications that show that equatorial Africa region has intense convective storms in all the seasons (Zipser et al. 2006) and the greater concentration of lightning hotspots (Albrecht et al. 2016). Moreover, if there is less charge accumulation and the charge layers are closer, the flashes will be less energetic (less charge transferred across smaller potential drop, see Figures 12 and 13), shorter and smaller. Additionally, in the results section we reported that aerosol concentration is larger in Africa (Figures 7-10). Wang et al. (2018) investigated the relation of atmospheric optical depth (AOD) with lighting rate in two regions of Africa, dust-dominant and smoke-dominant regions respectively, and showed that in both cases lightning flash rate peaks at AOD ≈ 0.3. Moreover, Fan et al. (2018) showed that ultrafine aerosol particles from pollution plumes ingested into deep convective intensify convective strength. Williams (2005a) proposed that a more polluted boundary layer would enhance electrification processes. Numerical models of thunderstorm electrification that takes into account the effects of aerosol support this hypothesis (Mansell and Ziegler 2013, Zhao et al. 2015). This strong electrification together with the elevated and more closely separated charge regions can explain high IC flash rates.

Here we have also observed that extreme values of 2-meter temperature in Africa are higher compared with CA what is consistent with Williams et al. (2005b) who reported a quasi-exponential dependence of flash rate with temperature. Thus, the characteristics reported here in the region of interest in Africa, may generate thunderstorms with elevated and closer charge regions and strong electrification, consequence of the strong deep convection and high aerosol concentration, as discussed by Matsui et al. (2016). This kind of thunderstorms are consistent with the MCS reported by Toracinta and Zipser (2001). We have inferred that these characteristics allow for higher IC flash rate but the flashes are less energetic, shorter and smaller. This is consistent with lightning properties measured by LIS and OTD by Beirle et al. (2014) who reported that flash rate is higher in Africa but flash energy, flash duration and flash extension are smaller compared to CA. The implications of the results discussed here on thunderstorm development, electrification process, charge structure, flash rate and flash characteristics are summarized in the Table 2.

There is another possibility that has to be taken into account. Strong updrafts may lead to situations with high turbulence that results in a complex organization with multiple blobs of charge like the charge structure proposed by Bruning and MacGorman (2013, figure 1.b). Bruning and MacGorman (2013) show that conditions for frequent lightning initiation and extensive propagation are opposed. This kind of complex structure can support large flash rates for small flashes. This situation is also consistent with the flash properties measured by LIS and OTD reported by Beirle et al. (2014) and previously discussed.

Cummer et al (2015) reported that leaders associated with TGFs are vertically oriented, quite long (2.7 - 4.5 km) and fast (0.8 -$1 \cdot 10^6$ m/s) and possibly accelerating with altitude. Cummer et al. (2015) also suggests that these flashes can possibly develop because of the existence of a very strong electric field and high potential difference between the main negative and the main positive charge region. In the Figures 12 and 13 we present the electric field and potential calculated in two different situations of the model presented previously. Figure 12 (case 1) shows the result of the numerical model with the conditions presented in the Table 1. Figure 13 (case 2) shows the result for a charge separation between main charge regions of 400 m and charge density reduced to the 71% of the values presented in Table 1, which is large enough to achieve lightning initiation for this charge separation as can be seen in Figure 9. Thunderstorms with large separation between the two main charge regions (figure 12) are the ones believed to be more common in CA, while thunderstorms with the main charge regions closer are the ones more common in Africa (figure 13).

We can see that the conditions suggested by Cummer et al. (2015) favorable to produce lightning linked to TGFs, namely strong electric field and potential drop, are achieved for greater separation between charge regions (Figure 12). This is also consistent with both TGF production mechanisms. The leader model (Moss et al., 2006, Dwyer,2008, Carlson et al., 2010, Dwyer et al., 2010, Celestin, 2012, Pasko 2014) requires a very strong electric field at the tip of a long leader. We have shown here, that longer and more energetic leaders occur for the case 1 represented in Figure 12 while the ones occurring in case 2 of Figure 13 are shorter and less energetic. Moreover, a recent publication by Skeltved et al. (2017) have calculated that with a potential difference of 240 MV between the lower and upper leader tips and other assumptions like horizontal branching in the main negative charge layer a fully developed RREA spectrum can be obtained. This is only consistent with the case 1 in the Figure 12.c, where the maximum potential difference between the lower and upper leader is 257 MV while for the case 2 in Figure 11.c is 161 MV. On the other hand, the feedback mechanism (Dwyer, 2012, Liu and Dwyer, 2013) requires large-scale thundercloud and lightning fields. Dwyer (2012) indicated the feedback mechanism requires at least potential differences of 100 MV to operate, and more typically 200 – 400 MV. It can be seen by comparing Figure 12.c and Figure 13.c that this condition is hardly achieved in the second one. All the conditions discussed above points out that TGFs can be hardly achieved for the case 2 in the Figure 13, which is the case of the thunderstorm vertical electric charge structure to be suggested to occur in Africa. This hypothesis is reinforced by the observations and reanalysis presented here in the previous section. It is known that CAPE is an important factor for TGF production (Splitt et al., 2010, Fabró et al., 2015). JJA is the only season that CAPE is clearly lower in Africa than in CA (Table 3). It can be seen in the Figure 9 that TGFs occurrence is low than one should expect in the region with the highest flash density in Central Africa. For the other seasons, CAPE is high in Africa in the regions with the highest flash density, but also is high the AOT (Figures 7, 8 and 10), and again TGF occurrence, in comparison with regions with lower CAPE and flash density is also lower than expected.

The discussion of the results we have presented here leads us to conclude that surface land type characteristics in Africa allow for the development of thunderstorms with elevated main negative charge region closer to the main positive charge region. That vertical structure favors larger IC flash rates, but these flashes are smaller, shorter and less energetic. According to the TGF production mechanism and analysis of flashes associated with TGFs, we conclude that the vertical structure of thunderstorms in Africa is less favorable for TGF production in comparison with CA may explain the TGF/lighting ratio asymmetry.

5 Summary

In this paper we have investigated if there are meteorological parameters that may explain the TGF/lightning asymmetry and therefore the comparatively weak TGF production in Africa:

- Drier surface and high CAPE in the region of interest in Africa allows for stronger updrafts which contribute to higher altitude electrical charge regions. Large concentrations of aerosols enhance electrification processes. These conditions suggest that thunderstorms in Africa may have intense electrification but charge regions are elevated in the atmosphere and closer to each other. Charge regions may also be more turbulent and less structured, producing frequent small discharges.
- We show through a very simple model of the vertical electric field and potential that this type of thunderstorm with closer and elevated charge regions requires less charge to achieve lightning initiation. This result allows for higher flash rates and less energetic, shorter and smaller flashes, a finding consistent with Beirle et al. (2014) and Bruning and MacGorman (2013)
- The result of the model for the electric field and potential for the case with elevated and closer charge regions shows that these thunderstorms, which are the ones suggested to occur in Africa, do not accomplish the favorable conditions for TGF production (strong electric field and potential drop, according to observations (Cummer et al., 2015) and production mechanism models (Moss et al. 2006, Dwyer 2008, Carlson et al. 2010, Dwyer et al. 2010, Celestin 2012, Dwyer 2012, Liu and Dwyer 2013, Skeltved et al., 2017)).

Acknowledgments, Samples, and Data

This work was supported by research grants from the Spanish Ministry of Economy and the European Regional Development Fund (FEDER): MINECO AYA2011-29936-C05-04 and (MINECO/FEDER) ESP2013- 48032-C5-3-R and (MINECO/FEDER) ESP2015-69909-C5-R

Data, methodology routines and the model for and developed for this paper are detailed in the Supporting Information document

References

Albrecht, R.I., Goodman, S.J., Buechler, D.E., Blakeslee, R.J. and Christian, H.J. , (2016): Where Are the Lightning Hotspots on Earth?. *Bulletin of American Meteorological Society*, **97**, 2051–2068

Barnes, D. E., M. E. Splitt, J. R. Dwyer, S. Lazarus, D. M. Smith, and H. K. Rassoul (2015): A study of thunderstorm microphysical properties and lightning flash counts associated with

terrestrial gamma-ray flashes. *Journal of Geophysical Research: Atmosphere*, **120**, 3453–3464.

Beirle, S., Koshak, W., Blakeslee, R., and Wagner, T. (2014): Global patterns of lightning properties derived by OTD and LIS. *Natural Hazards and Earth System Sciences* **14**, 2715–2726.

Briggs, M.S., Fishman, G.J., Connaughton, V., Bhat, P.N., Paciesas, W.S., Preece, R.D., Wilson-Hodge, C., Chaplin, V.L., Kippen, R.M., Von Kienlin, A., et al. (2010): First results on terrestrial gamma ray flashes from the Fermi Gamma-ray Burst Monitor. *Journal of Geophysical Research: Space Physics* **115**.

Briggs, M. S., et al. (2013): Terrestrial gamma-ray flashes in the Fermi era: Improved observations and analysis methods. *Journal of Geophysical Research: Space Physics.* **118**, 3805–3830.

Bruning, E.C. and D.R. MacGorman, 2013: Theory and Observations of Controls on Lightning Flash Size Spectra. *Journal of Atmospheric Sciences*, **70**, 4012–4029

Carlson, B.E., Lehtinen, N.G., and Inan, U.S. (2010): Terrestrial gamma ray flash production by active lightning leader channels. *Journal of Geophysical Research: Space Physics* **115**.

Cecil, D.J., D.E. Buechler, and R.J. Blakeslee (2015): TRMM LIS Climatology of Thunderstorm Occurrence and Conditional Lightning Flash Rates. *Journal of Climate,* **28**, 6536–6547

Celestin, S., and Pasko, V.P. (2011): Energy and fluxes of thermal runaway electrons produced by exponential growth of streamers during the stepping of lightning leaders and in transient luminous events. *Journal of Geophysical Research: Space Physics* **116**.

Christian, H. J., et al. (2003): Global frequency and distribution of lightning as observed from space by the Optical Transient Detector. *Journal of Geophysical Research*, **108(D1)**, 4005.

Connaughton, V., Briggs, M.S., Holzworth, R.H., Hutchins, M.L., Fishman, G.J., Wilson-Hodge, C.A., Chaplin, V.L., Bhat, P.N., Greiner, J., Von Kienlin, A., et al. (2010): Associations between Fermi Gamma-ray Burst Monitor terrestrial gamma ray flashes and sferics from the World Wide Lightning Location Network. *Journal of Geophysical Research: Space Physics* **115**.

Chronis, T., Briggs, M.S., Priftis, G., Connaughton, V., Brundell, J., Holzworth, R., Heckman, S., McBreen, S., Fitzpatrick, G., and Stanbro, M. (2016): Characteristics of thunderstorms that produce terrestrial gamma ray flashes. *Bulletin of the American Meteorological Society* **97**, 639–653.

Cummer, S.A., Zhai, Y., Hu, W., Smith, D.M., Lopez, L.I., and Stanley, M.A. (2005): Measurements and implications of the relationship between lightning and terrestrial gamma ray flashes. *Geophysical Research Letters* **32**, 1–5.

Cummer, S. A., M. S. Briggs, J. R. Dwyer, S. Xiong, V. Connaughton, G. J. Fishman, G. Lu, F. Lyu, and R. Solanki (2014): The source altitude, electric current, and intrinsic brightness of terrestrial gamma ray flashes. *Geophysical Research Letters*, **41**, 8586–8593.

Cummer, S. A., F. Lyu, M. S. Briggs, G. Fitzpatrick, O. J. Roberts, and J. R. Dwyer (2015): Lightning leader altitude progression in terrestrial gamma-ray flashes. *Geophysical Research Letters*, **42**, 7792–7798.

Dee, D.P., Uppala, S.M., Simmons, A.J., Berrisford, P., Poli, P., Kobayashi, S., Andrae, U., Balmaseda, M.A., Balsamo, G., Bauer, P., et al. (2011): The ERA-Interim reanalysis:

Configuration and performance of the data assimilation system. *Quarterly Journal of the Royal Meteorological Society* **137**, 553–597.

Dwyer, J.R. (2008): Source mechanisms of terrestrial gamma-ray flashes. *Journal of Geophysical Research Atmospheres* **113**.

Dwyer, J.R. (2012): The relativistic feedback discharge model of terrestrial gamma ray flashes. *Journal of Geophysical Research: Space Physics* **117**.

Dwyer, J.R., and Smith, D.M. (2005): A comparison between Monte Carlo simulations of runaway breakdown and terrestrial gamma-ray flash observations. *Geophysical Research Letters* **32**, 1–4.

Dwyer, J.R., Smith, D.M., Uman, M.A., Saleh, Z., Grefenstette, B., Hazelton, B., and Rassoul, H.K. (2010): Estimation of the fluence of high-energy electron bursts produced by thunderclouds and the resulting radiation doses received in aircraft. *Journal of Geophysical Research* **115**, D09206.

Fabró, F., Montanyà, J., Marisaldi, M., van der Velde, O.A., and Fuschino, F. (2015): Analysis of global Terrestrial Gamma Ray Flashes distribution and special focus on AGILE detections over South America. *Journal of Atmospheric and Solar-Terrestrial Physics* **124**, 10–20.

Fan, J., Rosenfeld, D., Zhang, Y., Giangrande, S. E., Li, Z., Machado, L. A. T., Martin, S. T., Yang, Y., Wang, J., Artaxo, P., Barbosa, H. M. J., Braga, R. C., Comstock, J. M., Feng, Z., Gao, W., Gomes, H. B., Mei, F., Pöhlker, C., Pöhlker, M. L., Pöschl, U. and de Souza, R. A. F. (2018): Substantial convection and precipitation enhancements by ultrafine aerosol particles. *Science*, **359**(6374), 411-418.

Fuschino, F., Marisaldi, M., Labanti, C., Barbiellini, G., Del Monte, E., Bulgarelli, A., Trifoglio, M., Gianotti, F., Galli, M., Argan, A., et al. (2011): High spatial resolution correlation of AGILE TGFs and global lightning activity above the equatorial belt. *Geophysical Research Letters* **38**.

Guo F. X., Lu G. Y., Wu X., Wang H. L., Liu Z. P., Bao M., Li Y. W. (2016): Occurrence conditions of positive cloud-to-ground flashes in severe thunderstorms. *Science China Earth Sciences*, **59**, 1401–1413.

Karlsson, K.-G., Riihelä, A., Müller, R., Meirink, J. F., Sedlar, J., Stengel, M., Lockhoff, M., Trentmann, J., Kaspar, F., Hollmann, R., and Wolters, E. (2016): CLARA-A1: a cloud, albedo, and radiation dataset from 28 yr of global AVHRR data, *Atmospheric Chemistry and Physics*, **13**, 5351-5367.

Krehbiel, P. R., Riousset, J. A., Pasko, V. P., Thomas, R. J., Rison, W., Stanley, M. A., Edens, H. E. (2008): Upward electrical discharges from thunderstorms, *Nature Geoscience*, **1,** 233.

Liu, C., and Zipser, E. J. (2005): Global distribution of convection penetrating the tropical tropopause, *Journal of Geophysical Research*, **110**, D23104.

Liu, C., Zipser, E.J., Cecil, D.J., Nesbitt, S.W. and Sherwood, S. (2008): A Cloud and Precipitation Feature Database from Nine Years of TRMM Observations. *Journal of Applied Meteorology and Climatology*, **47**, 2712–2728.

Liu, N., and Dwyer, J.R. (2013): Modeling terrestrial gamma ray flashes produced by relativistic feedback discharges. *Journal of Geophysical Research: Space Physics* **118**, 2359–2376.

López, J.A., J. Montanyà, N. Pineda, O. A. van der Velde, A. Salvador, D. Romero, D. Aranguren, J. Taborda (2018): Charge structure of two tropical thunderstorms in Colombia. *Journal of Geophysical Research: Atmospheres,* DOI: 10.1029/2018JD029188

Lu, G., Blakeslee, R.J., Li, J., Smith, D.M., Shao, X.M., McCaul, E.W., Buechler, D.E., Christian, H.J., Hall, J.M., and Cummer, S.A. (2010): Lightning mapping observation of a terrestrial gamma-ray flash. *Geophysical Research Letters* **37**.

MacGorman, D.R., D.W. Burgess, V. Mazur, W.D. Rust, W.L. Taylor, and B.C. Johnson (1989): Lightning Rates Relative to Tornadic Storm Evolution on 22 May 1981. *Journal of the Atmospheric Sciences,* **46**, 221–251.

Mansell, E.R. and C.L. Ziegler (2013): Aerosol Effects on Simulated Storm Electrification and Precipitation in a Two-Moment Bulk Microphysics Model. *Journal of the Atmospheric Sciences,* **70**, 2032–2050

Marisaldi, M., Fuschino, F., Labanti, C., Galli, M., Longo, F., Del Monte, E., Barbiellini, G., Tavani, M., Giuliani, A., Moretti, E., et al. (2010): Detection of terrestrial gamma ray flashes up to 40 MeV by the AGILE satellite. *Journal of Geophysical Research: Space Physics* **115**.

Marshall, T. C., W. D. Rust, and M. Stolzenburg (1995): Electrical structure and updraft speeds in thunderstorms over the southern Great Plains, *Journal of Geophysical Research*, **100**(D1), 1001–1015.

Matsui, T., Chern, J., Tao, W., Lang, S., Satoh, M., Hashino, T. and Kubota, T., (2016): On the Land–Ocean Contrast of Tropical Convection and Microphysics Statistics Derived from TRMM Satellite Signals and Global Storm-Resolving Models. *Journal of Hydrometeorology*, **17**, 1425–1445.

Meyer, K., Yang, P. and Gao, B.C., (2007): Tropical ice cloud optical depth, ice water path, and frequency fields inferred from the MODIS level-3 data. *Atmospheric Research*, **85(2)**, 171-182.

Moss, G.D., Pasko, V.P., Liu, N., and Veronis, G. (2006): Monte Carlo model for analysis of thermal runaway electrons in streamer tips in transient luminous events and streamer zones of lightning leaders. *Journal of Geophysical Research: Space Physics,* **111**.

Østgaard, N., T. Gjesteland, J. Stadsnes, P. H. Connell, and B. Carlson (2008): Production altitude and time delays of the terrestrial gamma flashes: Revisiting the Burst and Transient Source Experiment spectra, *Journal of Geophysical Research*, **113**, A02307

Østgaard, N., T. Gjesteland, B. E. Carlson, A. B. Collier, S. A. Cummer, G. Lu, and H. J. Christian (2013): Simultaneous observations of optical lightning and terrestrial gamma ray flash from space. *Geophysical Research Letters*, **40** , 2423–2426.

Pasko, V. P. (2014), Electrostatic modeling of intracloud stepped leader electric fields and mechanisms of terrestrial gamma ray flashes, *Geophysical Research Letters*, **41**, 179–185

Riousset, J. A., V. P. Pasko, P. R. Krehbiel, R. J. Thomas, and W. Rison (2007): Three-dimensional fractal modeling of intracloud lightning discharge in a New Mexico thunderstorm and comparison with lightning mapping observations. *Journal of Geophysical Research*, **112**, D15203.

Rodger, C.J., Werner, S., Brundell, J.B., Lay, E.H., Thomson, N.R., Holzworth, R.H., and Dowden, R.L. (2006): Detection efficiency of the VLF World-Wide Lightning Location Network (WWLLN): Initial case study. *Annales Geophysicae* **24**, 3197–3214.

Shao, X.M., Hamlin, T., and Smith, D.M. (2010): A closer examination of terrestrial gamma-ray flash-related lightning processes. *Journal of Geophysical Research: Space Physics* **115**.

Skeltved, A. B., N. Østgaard, A. Mezentsev, N. Lehtinen, and B. Carlson (2017), Constraints to do realistic modeling of the electric field ahead of the tip of a lightning leader, *Journal of Geophysical Research: Atmospheres*, **122**, 8120–8134

Smith, D.M., Lopez, L.I., Lin, R.P., and Barrington-Leigh, C.P. (2005): Terrestrial gamma-ray flashes observed up to 20 MeV. *Science* **307**, 1085–1088.

Smith, D.M., Hazelton, B.J., Grefenstette, B.W., Dwyer, J.R., Holzworth, R.H., and Lay, E.H. (2010): Terrestrial gamma ray flashes correlated to storm phase and tropopause height. *Journal of Geophysical Research: Space Physics* **115**.

Splitt, M.E., Lazarus, S.M., Barnes, D., Dwyer, J.R., Rassoul, H.K., Smith, D.M., Hazelton, B., and Grefenstette, B. (2010): Thunderstorm characteristics associated with RHESSI identified terrestrial gamma ray flashes. *Journal of Geophysical Research: Space Physics* **115**.

Stanley, M.A., Shao, X.M., Smith, D.M., Lopez, L.I., Pongratz, M.B., Harlin, J.D., Stock, M., and Regan, A. (2006): A link between terrestrial gamma-ray flashes and intracloud lightning discharges. *Geophysical Research Letters* **33**.

Stolzenburg, M., W. D. Rust, and T. C. Marshall (1998): Electrical structure in thunderstorm convective regions: 3. Synthesis, *Journal of Geophysical Research*, **103**(D12), 14097–14108.

Tavani, M., Marisaldi, M., Labanti, C., Fuschino, F., Argan, A., Trois, A., Giommi, P., Colafrancesco, S., Pittori, C., Palma, F., et al. (2011): Terrestrial gamma-ray flashes as powerful particle accelerators. *Physical Review Letters* **106**.

Toracinta, E.R. and E.J. Zipser, (2001): Lightning and SSM/I-Ice-Scattering Mesoscale Convective Systems in the Global Tropics. *Journal of applied Meteorology*, 40, 983–1002.

Wang, Q., Li, Z., Guo, J., Zhao, C., and Cribb, M. (2018): The climate impact of aerosols on the lightning flash rate: is it detectable from long-term measurements?. *Atmospheric Chemistry and Physics*, **18**, 12797-12816.

Williams, E.R. (2005a): Lightning and climate: A review. *Atmospheric Research* **76**, 1–4, 272-287.

Williams, E.R., Mushtak, V.C., Rosenfeld, D., Goodman, S.J., Boccippio, D.J., (2005b): Thermodynamic conditions favorable to superlative thunderstorm updraft, mixed phase microphysics and lightning flash rate. *Atmospheric Research*. **76**, 288–306

Williams, E., Boldi, R., Bór, J., Sátori, G., Price, C., Greenberg, E., Takahashi, Y., Yamamoto, K., Matsudo, Y., Hobara, Y., et al. (2006): Lightning flashes conducive to the production and escape of gamma radiation to space. *Journal of Geophysical Research Atmospheres* **111**.

Zipser, E.J., Cecil, D.J., Liu, C., Nesbitt, S.W. and Yorty, D.P., (2006): Where are the most intense thunderstorms on Earth. *Bulletin of American Meteorological Society*, **87**, 1057–1072

Zhao, P., Yin, Y., Xiao, H. (2005): The effects of aerosol on development of thunderstorm electrification: A numerical study. *Atmospheric Research*, **153**, 376-391.

Table 1. Summary of the median and 90th percentile values calculated for the three regions analyzed.

	$P_{Af}50$	$P_{CA}50$	$P_{Af}90$	$P_{CA}90$
2-meter temperature (K)	297	299	306	306
CAPE (J/kg)	1096	1007	1998	1862
TCLW (kg/kg)	0.024	0.044	0.108	0.150
TCIW (kg/kg)	0.006	0.010	0.054	0.070
TCWV (kg/kg)	32	43	47	54

Table 2. Summary of the median and 90th percentile values calculated for the three regions analyzed in the periods DJF and MAM

	DJF				**MAM**			
	$P_{Af}50$	**$P_{CA}50$**	**$P_{Af}90$**	**$P_{CA}90$**	**$P_{Af}50$**	**$P_{CA}50$**	**$P_{Af}90$**	**$P_{CA}90$**
2-meter temperature (K)	298	299	309	303	298	299	310	304
CAPE (J/kg)	1136	855	2204	1534	1202	993	2166	1787
TCLW (kg/kg)	0.015	0.034	0.092	0.144	0.025	0.041	0.107	0.153
TCIW (kg/kg)	0.003	0.003	0.038	0.049	0.009	0.012	0.060	0.074
TCWV (kg/kg)	23	38	40	51	36	44	55	55

Table 3. Summary of the median and 90th percentile values calculated for the three regions analyzed in the periods JJA and SON

	JJA				**SON**			
	$P_{Af}50$	**$P_{CA}50$**	**$P_{Af}90$**	**$P_{CA}90$**	**$P_{Af}50$**	**$P_{CA}50$**	**$P_{Af}90$**	**$P_{CA}90$**
2-meter temperature (K)	296	298	303	303	297	299	303	303
CAPE (J/kg)	881	1087	1541	2123	1081	1073	1897	1954
TCLW (kg/kg)	0.024	0.056	0.105	0.166	0.033	0.052	0.119	0.149
TCIW (kg/kg)	0.004	0.016	0.040	0.082	0.011	0.017	0.063	0.076
TCWV (kg/kg)	29	46	46	54	37	47	49	56

Table 3. Summary of the implication on thunderstorm development, electrification process and charge structure parameters due to analyzed results in Section 3 and lightning flash characteristics in the three regions compared.

Parameter	**Observation in Africa's region of interest**	**Implication**
CAPE (Fig. 2.a-b)	$P_{Af}50 > P_{SA}50, P_{SeA}50$ $P_{Af}90 > P_{SA}90, P_{SeA}90$	Stronger updraft favored over Africa
Water content (Fig. 4,5,6.a-b)	$P_{Af}50 < P_{SA}50, P_{SeA}50$ $P_{Af}90 < P_{SA}90, P_{SeA}90$	Stronger updraft favored over Africa
2-meter temperature (Fig. 3.a-b)	$P_{Af}50 > P_{SA}50, P_{SeA}50$ $P_{Af}90 > P_{SA}90, P_{SeA}90$	Larger flash rate favored over Africa
Atmospheric Optical Thickness and (Fig. 7.a-b) Carbon monoxide concentration(Fig. 8.a-b)	Af > SA, SeA	Electrification efficiency enhancement in African thunderstorms
Flash rate (Beirle et al. 2014)	Af > SA, SeA	Lightning initiation quickly achieved in African thunderstorms
Flash energy (Beirle et al. 2014)	Af < SA, SeA	Less charge in African thunderstorms
Flash duration (Beirle et al. 2014)	Af < SA, SeA	Charge regions in closer proximity or less extensive in African thunderstorms
Flash length (Beirle et al. 2014)	Af < SA, SeA	Charge regions in closer proximity or less extensive in African thunderstorms

Table 4. Altitude, radius, depth and electric charge of the four charge regions of the thundercloud model (based on Riousset et al., 2007, Krehbiel, 2008 and López et al., 2018).

Charge layer	Altitude (km)	Radius (km)	Depth (km)	Charge (C)
Lower positive	4.25	1.5	0.7	1.39
Main negative	6.5	3	3	-24.5
Main positive	11.9	4	4	23.1
Upper negative (screening layer)	14.3	4	0.2	-1.39

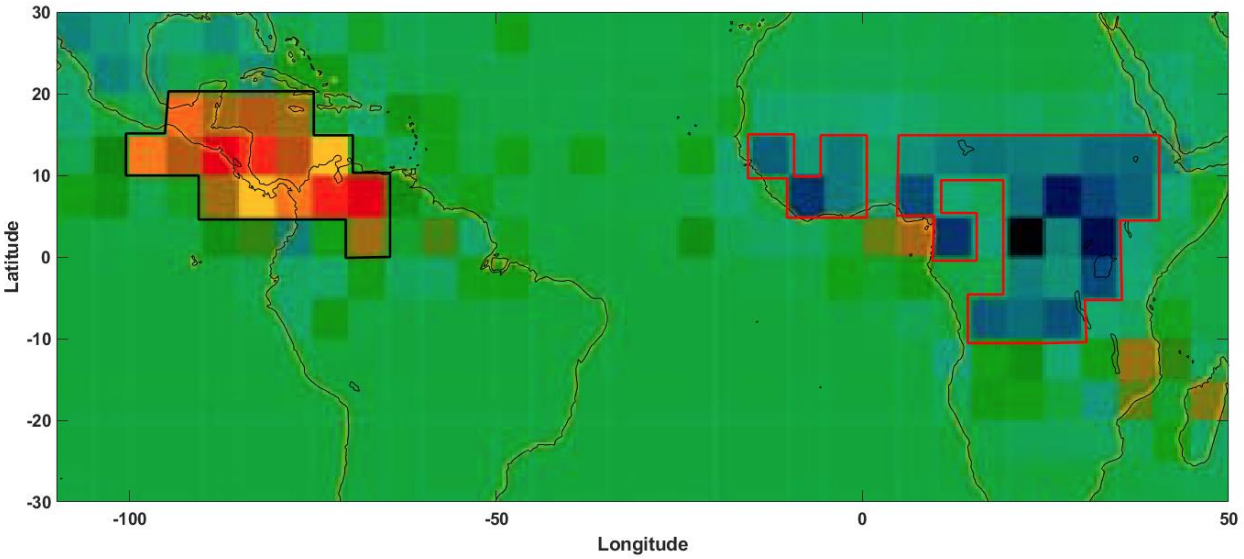

Figure 1. Regions with TGF/lightning ratio excess (black line) and TGF/lightning ratio deficit (red line). Adapted from Figure 5.d from Smith et al. (2010).

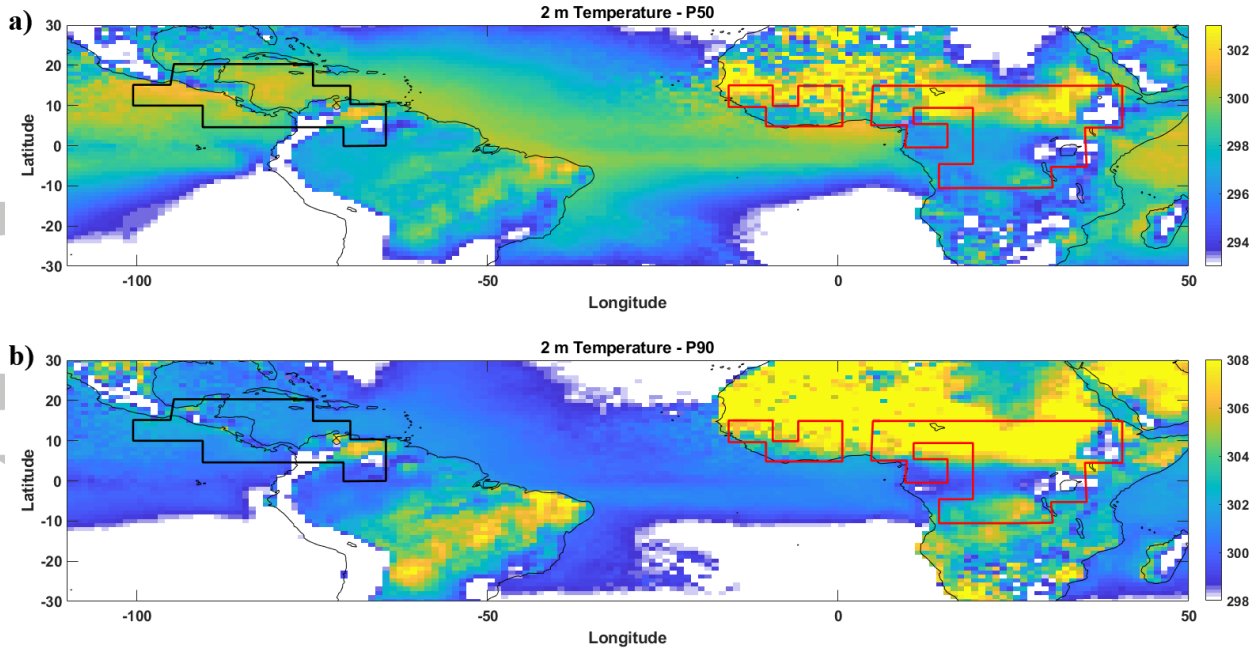

Figure 2. Median (a) and 90th percentiles (b) values of 2-meter temperature (K) for the 6-hour time periods with thunderstorm occurrence in 2010-2013. Regions with TGF/lightning ratio excess are enclosed with the black line while TGF/lightning ratio deficit are enclosed with the red line. The regions that are white are locations with values below the scale bar.

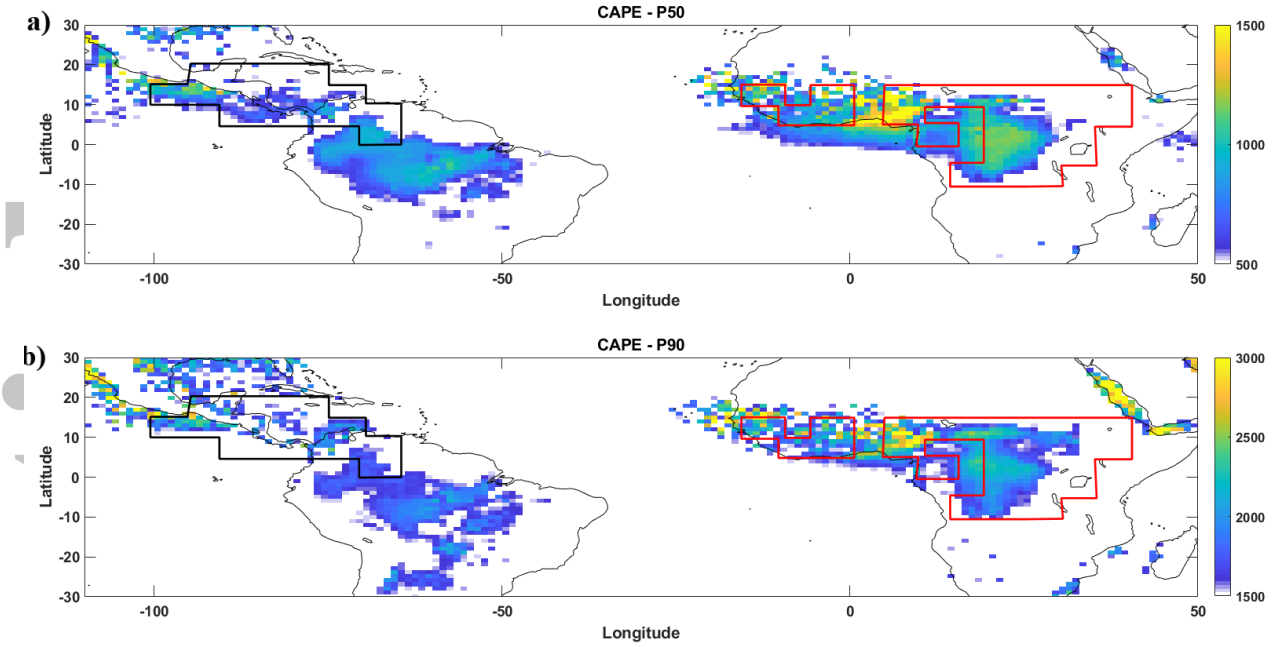

Figure 3. Median (a) and 90th percentile (b) values of CAPE (J/kg) for the 6-hour time periods with thunderstorm occurrence in 2010-2013. Regions with TGF/lightning ratio excess are enclosed with the black line while TGF/lightning ratio deficit are enclosed with the red line. The regions that are white are locations with values below the scale bar.

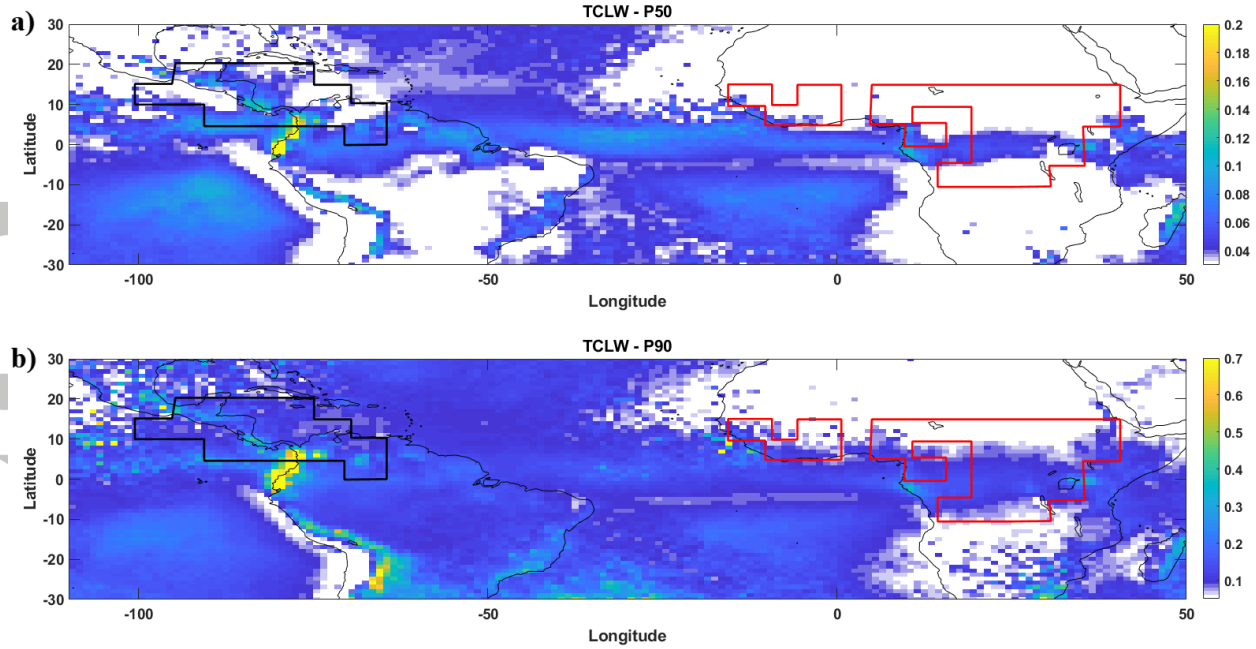

Figure 4. Median (a) and 90th percentile (b) values of Total column Liquid Water content (kg/kg) for the 6-hour time periods with thunderstorm occurrence in 2010-2013. Regions with TGF/lightning ratio excess are enclosed with the black line while TGF/lightning ratio deficit are enclosed with the red line. The regions that are white are locations with values below the scale bar.

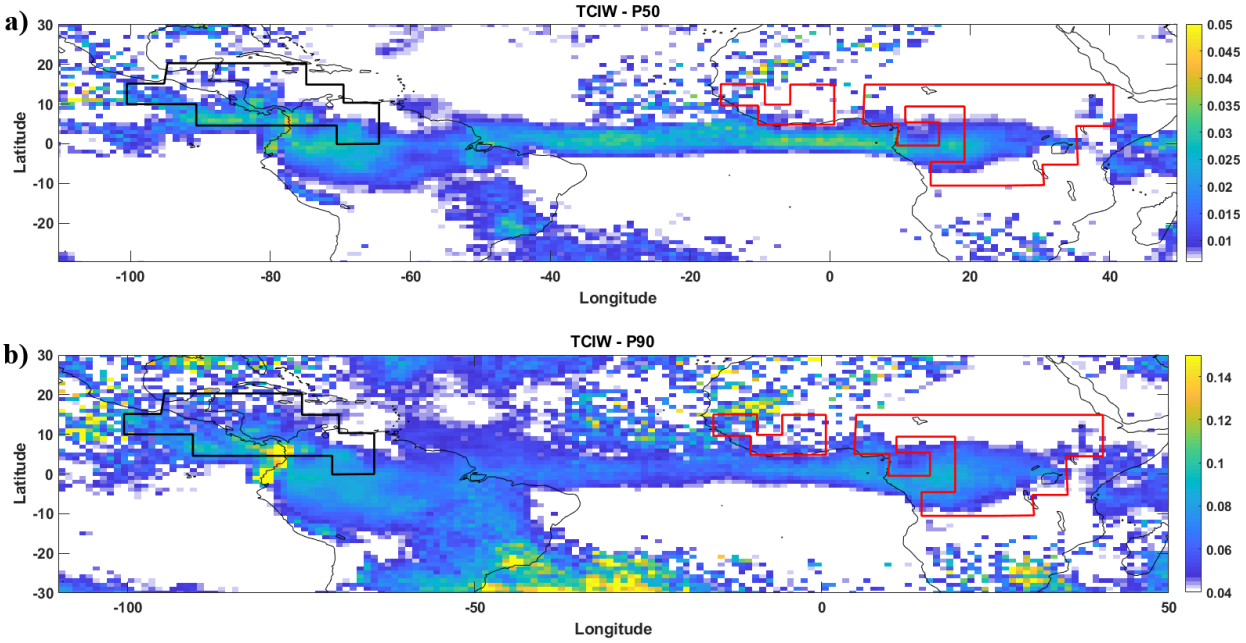

Figure 5. Median (a) and 90th percentile (b) values of Total column Ice Water content (kg/kg) for the 6-hout time periods with thunderstorm occurrence in 2010-2013. Regions with TGF/lightning ratio excess are enclosed with the black line while TGF/lightning ratio deficit are enclosed with the red line. The regions that are white are locations with values below the scale bar.

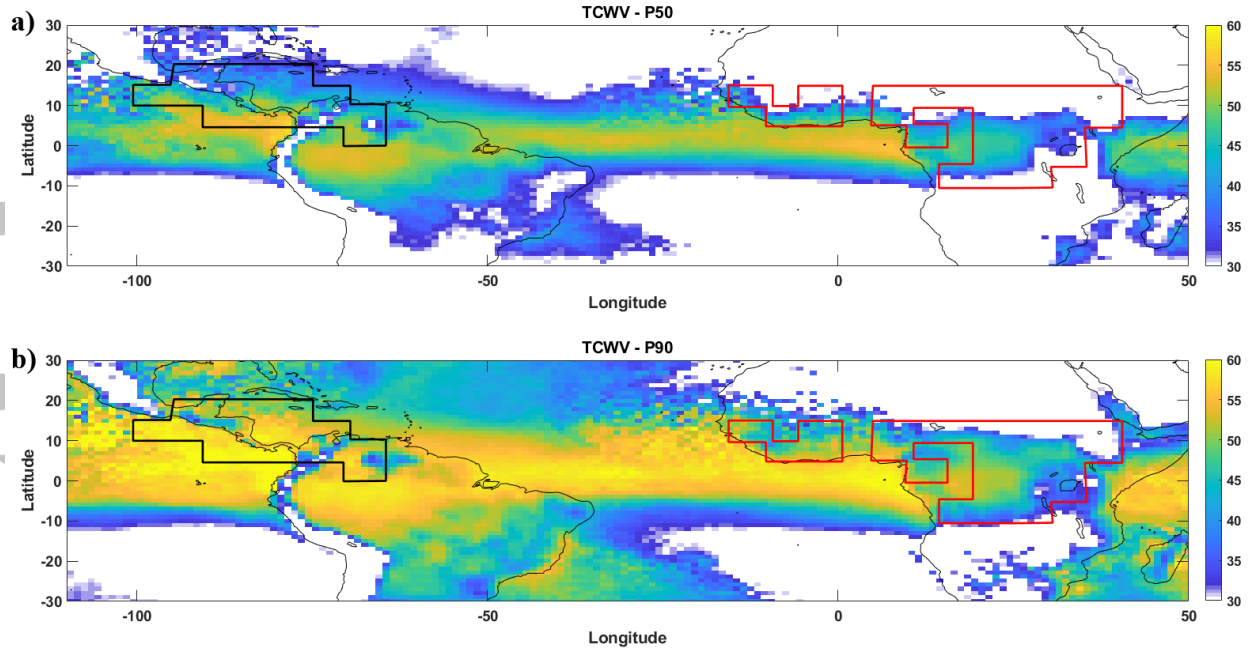

Figure 6. Median (a) and 90th percentile (b) values of Total column Water Vapor content (kg/kg) for the 6-hour time periods with thunderstorm occurrence in 2010-2013. Regions with TGF/lightning ratio excess are enclosed with the black line while TGF/lightning ratio deficit are enclosed with the red line. The regions that are white are locations with values below the scale bar.

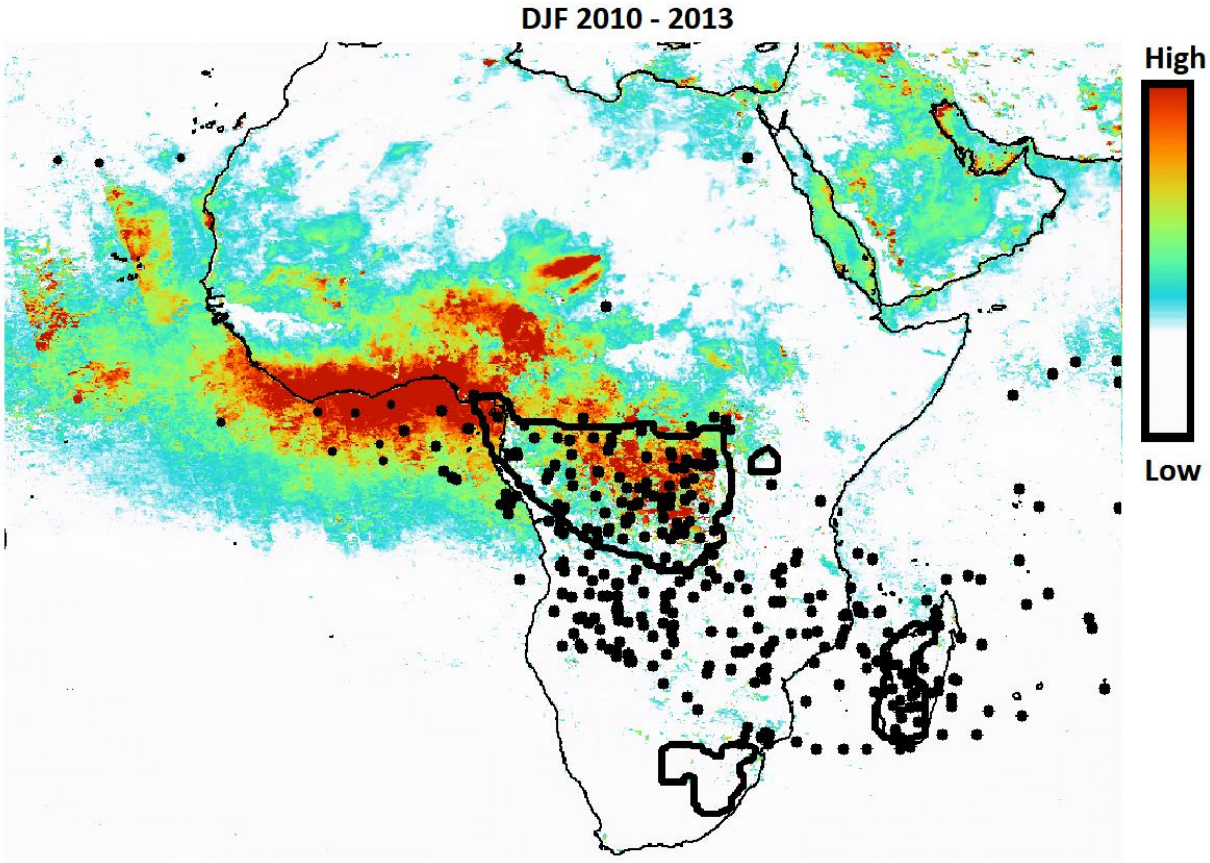

Figure 7. Atmospheric optical thickness (normalized units) for the DJF season for the period 2010 – 2013, TGFs detected by Fermi from 2008 to 2016 (black dots) and regions with TRMM LIS flash density > 40 flashes/km^2·year in the period 1998 – 2013 (black lines). Fermi TGFs and TRMM LIS flash rates are also for the DJF season.

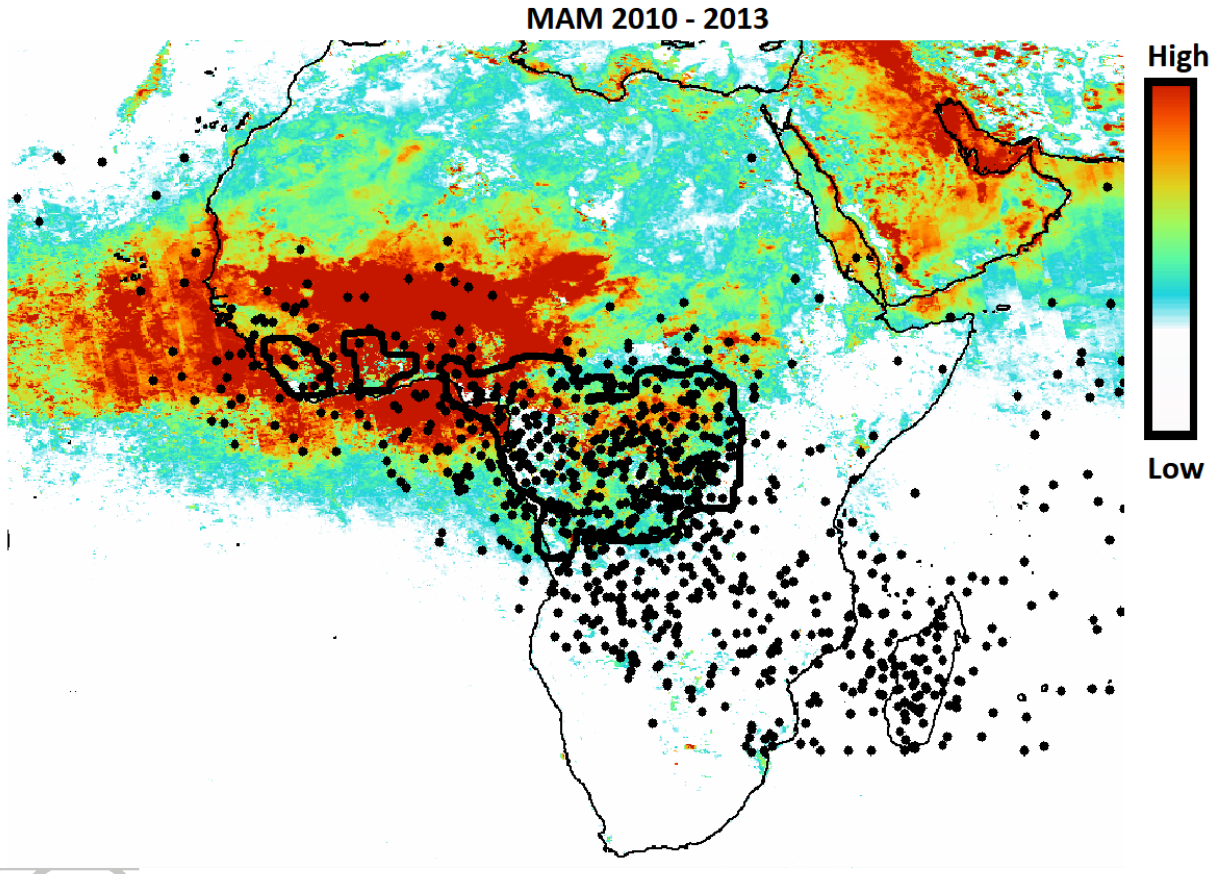

Figure 8. Atmospheric optical thickness (normalized units) for the MAM season for the period 2010 – 2013, TGFs detected by Fermi from 2008 to 2016 (black dots) and regions with TRMM LIS flash density > 40 flashes/km^2·year in the period 1998 – 2013 (black lines). Fermi TGFs and TRMM LIS flash density are also for the DJF season.

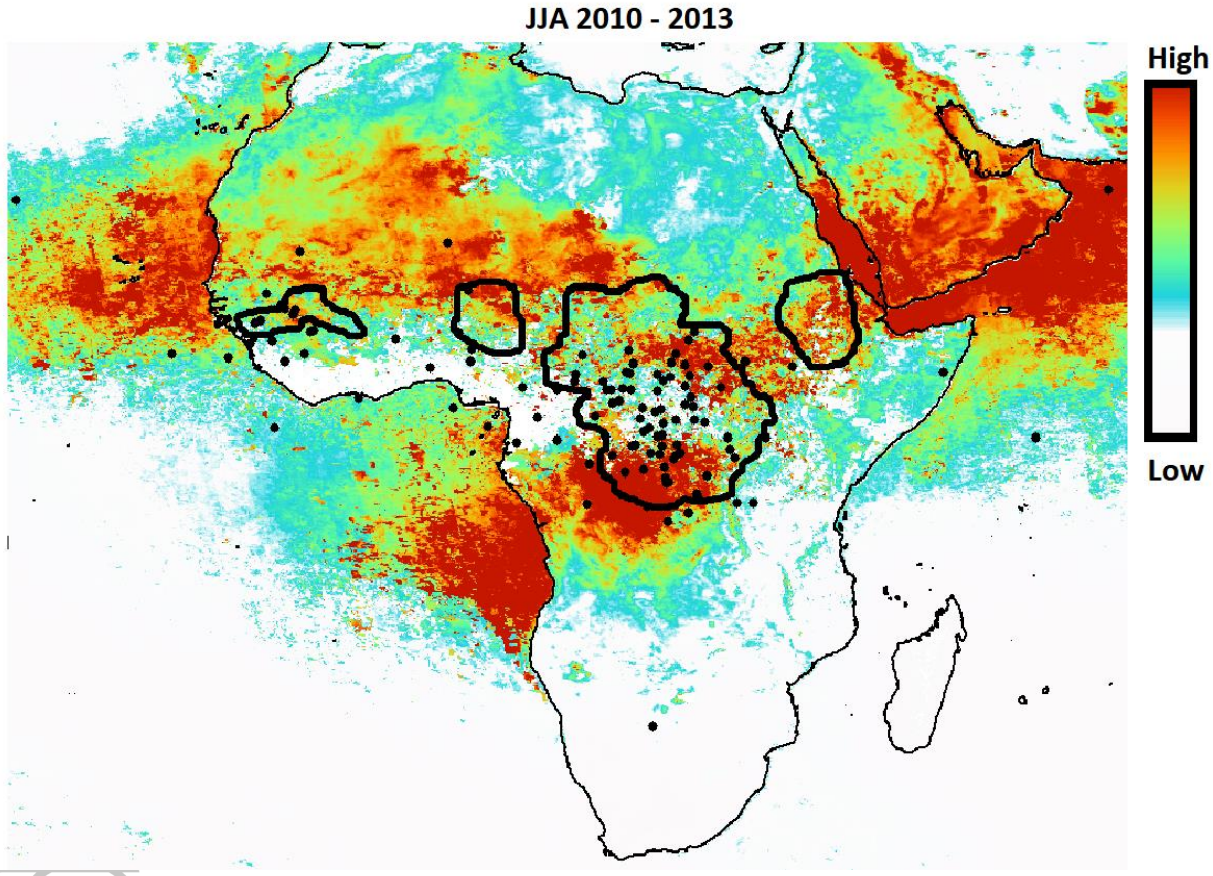

Figure 9. Atmospheric optical thickness (normalized units) for the JJA season for the period 2010 – 2013, TGFs detected by Fermi from 2008 to 2016 (black dots) and regions with TRMM LIS flash density > 40 flashes/km^2·year in the period 1998 – 2013 (black lines). Fermi TGFs and TRMM LIS flash density are also for the DJF season.

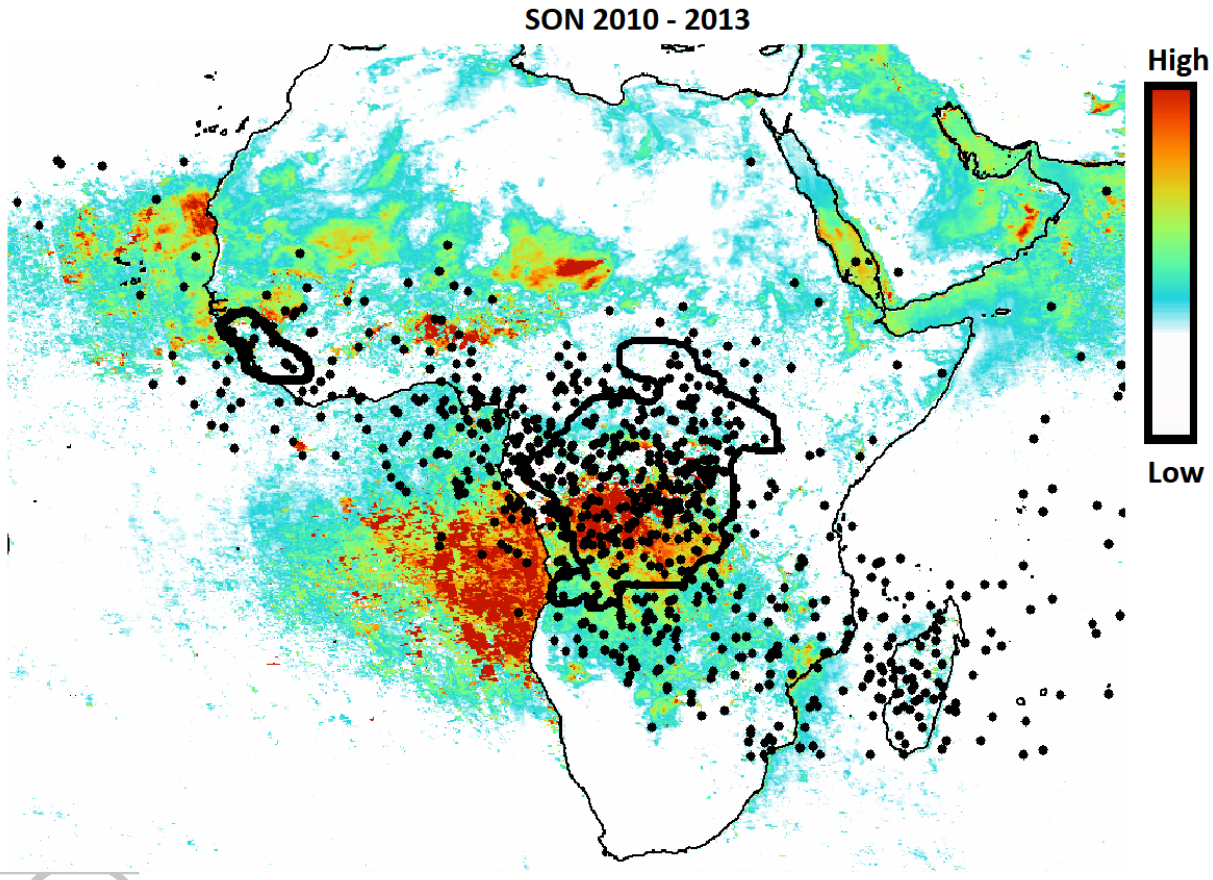

Figure 10. Atmospheric optical thickness (normalized units) for the SON season for the period 2010 – 2013, TGFs detected by Fermi from 2008 to 2016 (black dots) and regions with TRMM LIS flash density > 40 flashes/km^2·year in the period 1998 – 2013 (black lines). Fermi TGFs and TRMM LIS flash density are also for the DJF season.

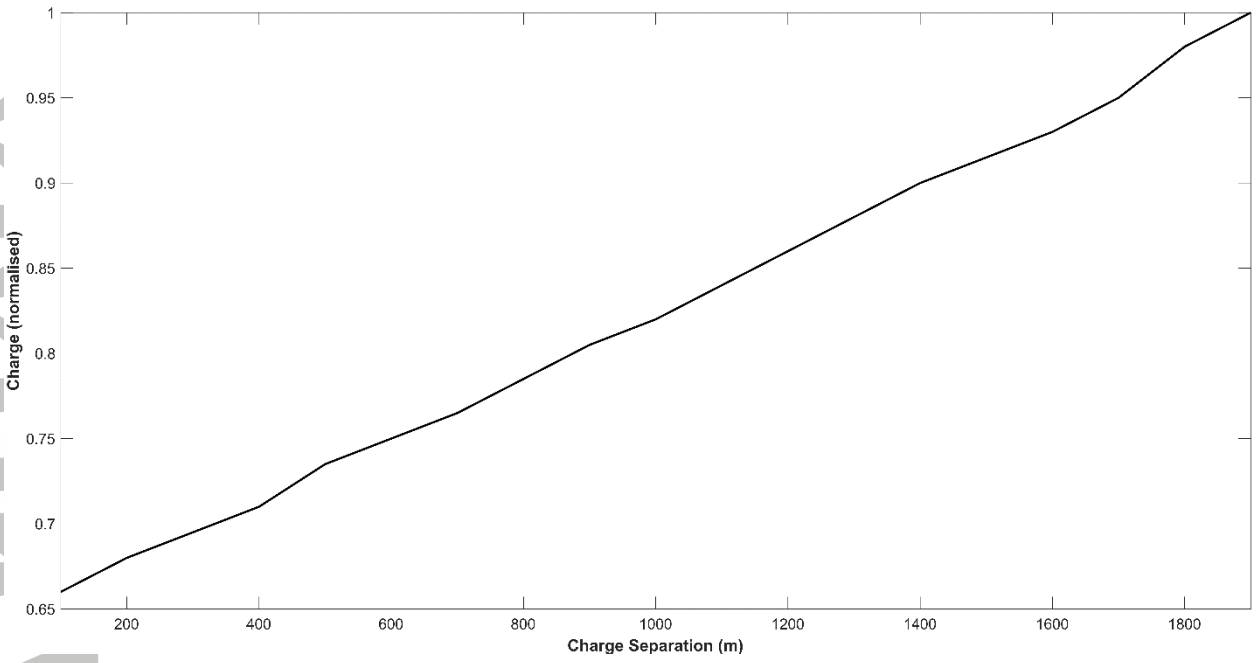

Figure 11. Charge needed to achieve lightning initiation as a function of the separation between the main negative and the main positive charge regions. Charge units are normalized to the charge in Table 4.

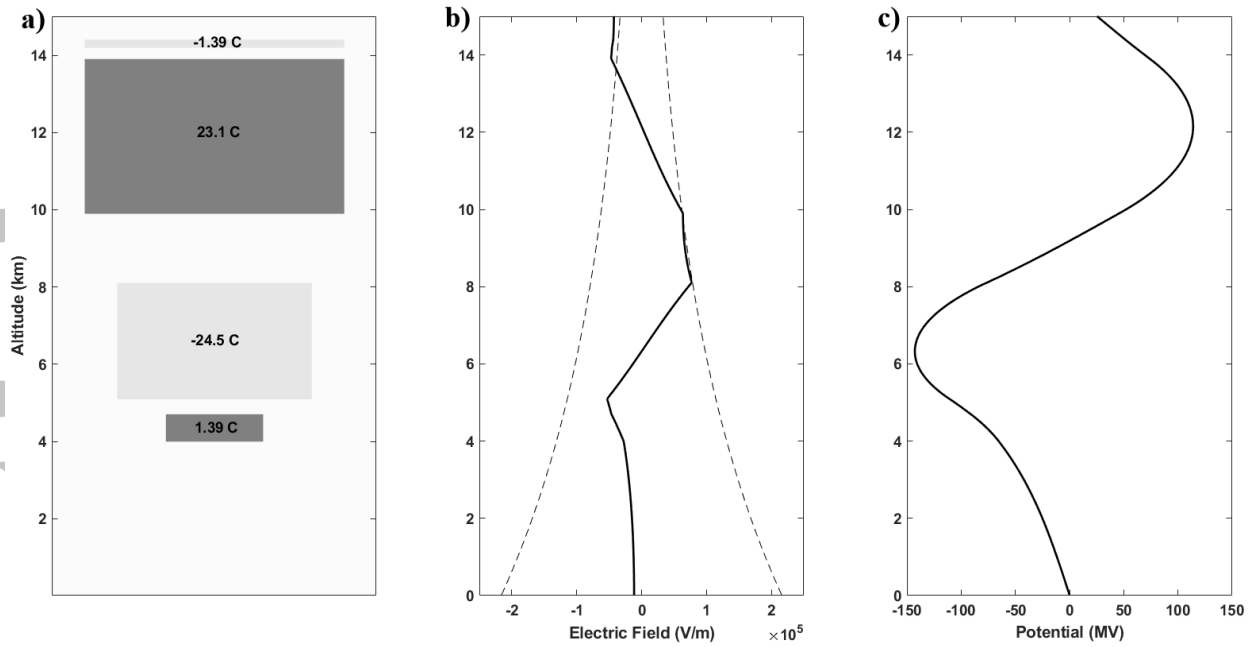

Figure 12. Case 1 **a)** Vertical charge distribution described in table 1. **b)** Vertical electric field. **c)** Vertical electric potential

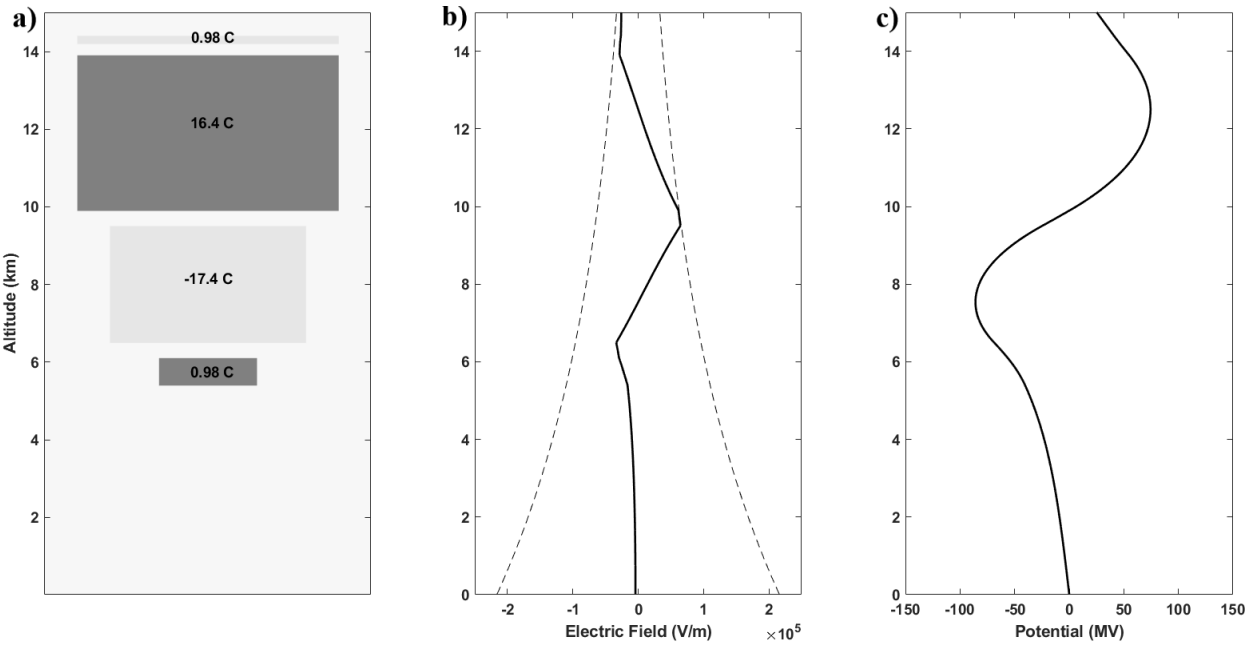

Figure 13. Case 2 **a)** Vertical charge distribution. Lower positive and main negative charge regions are 1.1 km elevated respect case 1. Charge density has been reduced to 64 % of values in table 1. **b)** Vertical electric field. **c)** Vertical electric potential